JOURNAL OF COMPUTATIONAL PHYSICS 113, 122-133 (1994)

Radiation Boundary Condition and Anisotropy Correction for Finite Difference Solutions of the Helmholtz Equation

CHRISTOPHER K. W. TAM AND JAY C. WEBB

Department of Mathematics, Florida State University, Tallahassee, Florida 32306-3027

Received March 9, 1992

In this paper finite-difference solutions of the Helmholtz equation in an open domain are considered. By using a second-order central difference scheme and the Bayliss–Turkel radiation boundary condition, reasonably accurate solutions can be obtained when the number of grid points per acoustic wavelength used is large. However, when a smaller number of grid points per wavelength is used excessive reflections occur which tend to overwhelm the computed solutions. Excessive reflections are due to the incompability between the governing finite difference equation and the Bayliss–Turkel radiation boundary condition. The Bayliss–Turkel radiation boundary condition was developed from the asymptotic solution of the partial differential equation. To obtain compatibility, the radiation boundary condition should be constructed from the asymptotic solution of the finite difference equation instead. Examples are provided using the improved radiation boundary condition based on the asymptotic solution of the governing finite difference equation. The computed results are free of reflections even when only five grid points per wavelength are used. The improved radiation boundary condition has also been tested for problems with complex acoustic sources and sources embedded in a uniform mean flow. The present method of developing a radiation boundary condition is also applicable to higher order finite difference schemes. In all these cases no reflected waves could be detected. The use of finite difference approximation inevitably introduces anisotropy into the governing field equation. The effect of anisotropy is to distort the directional distribution of the amplitude and phase of the computed solution. It can be quite large when the number of grid points per wavelength used in the computation is small. A way to correct this effect is proposed. The correction factor developed from the asymptotic solutions is source independent and, hence, can be determined once and for all. The effectiveness of the correction factor in providing improvements to the computed solution is demonstrated in this paper.

1. INTRODUCTION

This work is motivated by the need to perform direct numerical simulation of aeroacoustics problems. Aeroacoustics is the branch of science which deals with the generation and propagation of aircraft noise. Aicraft noise consists of both broadband and discrete components. Broadband components such as jet and airframe noise involve a large range of acoustic frequencies and wavelengths. Others such as propeller noise involve discrete tones of very high frequencies. To be able to deal with this class of problems it is imperative to use a computation scheme which can resolve waves of very short wavelengths. For a sinusoidal wave a minimum of about five grid points is required to define the waveform. Here our goal is to examine the feasibility of obtaining accurate finite difference acoustic wave solutions using as few as five grid points per acoustic wavelength.

Most aeroacoustic problems are exterior open domain problems. In practice, a finite computational domain is employed. This necessitates the imposition of a radiation boundary condition at the artificial boundaries of the computational domain. Numerous papers have been written now on the subject of radiation boundary conditions. Nevertheless, few appear to have investigated the applicability of their proposed radiation boundary condition to cases where the wavelength is only five to six times the spacing of the grid points. Bayliss, Turkel, and coworkers [1–3] developed a family of radiation boundary conditions for the simple wave equation and the Helmholtz equation, based on the far field asymptotic solution of the governing partial differential equation. The premise is that in the far field the computed solution must have the same form as the asymptotic solution. Engquist and Majda [4, 5] used a pseudo-differential operator technique to construct absorbing boundary conditions for this class of problems. The absorbing boundary condition minimizes the reflected waves off the artificial boundary of the computation domain. This idea has since been refined by Higdon [6, 7] and most recently generalized by Jiang and Wong [8]. Kosloff and Kosloff [9] proposed the incorporation of an artificial damping layer as absorbing boundaries for wave propagation problems. The basic idea of their method, largely motivated by physical considerations, is consistent with the thinking of Engquist and Majda. Aside from the above methods a number of investigators formulated radiating boundary conditions by means of the characteristics of the governing partial differential equations. The

0021-9991/94 $6.00

most recent works in this category are given by Thompson [10, 11].

In the absence of a mean flow, acoustic waves are governed by the simple wave equation. If the sources of sound have a discrete frequency, then by separating out time (with $e^{-i\omega t}$ dependence) the acoustic wave equation reduces to the Helmholtz equation

$$\nabla^2 p + k^2 p = f, \tag{1}$$

where p is the pressure perturbation, ∇^2 is the Laplacian operator, and f is the source distribution; k, the wave number, is equal to $2\pi/\lambda$, where λ is the acoustic wavelength. k is related to the angular frequency of the wave ω and speed of sound a_0 by $k = \omega/a_0$. If the problem is two-dimensional and f is a source localized at the origin, i.e.,

$$f = -\delta(x)\,\delta(y), \tag{2}$$

the solution of (1) satisfying an outgoing wave condition in the far field is

$$p = \frac{i}{4} H_0^{(1)}(kr), \qquad r = (x^2 + y^2)^{1/2}, \tag{3}$$

where $H_0^{(1)}$ is the zeroth-order Hankel function of the first kind. It is to be noted for later reference that $|p|$ of (3) is a monotonically deceasing function of x and that contours of equal sound intensity of $|p|$ are circles in the $x - y$ plane.

Suppose (1) is discretized using second-order central difference approximation with grid spacing Δx and Δy in the x and y directions, respectively; then the governing finite difference equation for $p_{m,n}$ (m, n are the indices in the x and y directions) is

$$\frac{p_{m+1,n} - 2p_{m,n} + p_{m-1,n}}{(\Delta x)^2} + \frac{p_{m,n+1} - 2p_{m,n} + p_{m,n-1}}{(\Delta y)^2} + k^2 p_{m,n} = f_{m,n}. \tag{4a}$$

Upon multiplying by $(\Delta y)^2$ the equation becomes

$$(p_{m+1,n} - 2p_{m,n} + p_{m-1,n})\left(\frac{\Delta y}{\Delta x}\right)^2 + (p_{m,n+1} - 2p_{m,n} + p_{m,n-1}) + (k\,\Delta y)^2 p_{m,n} = f_{m,n}(\Delta y)^2. \tag{4b}$$

The quantity $k\,\Delta y = 2\pi\,\Delta y/\lambda$, which is equal to 2π divided by the number of grid points per acoustic wavelength in the y direction, is an intrinsic parameter of the governing finite difference equation. It is, however, not a parameter of the Helmholtz equation which difference equation (4) tries to simulate. For simplicity unless otherwise stated Δx and Δy will be taken to be equal in this paper. To solve (4) in a finite computational domain a radiation boundary condition is needed. The Helmholtz equation has no characteristics so a direct application of the characteristic radiation boundary condition [10, 11] does not seem to be appropriate. The absorbing boundary conditions [4–8] which are predicated on minimizing reflections to the interior of the computational domain do not guarantee that the solution is not distorted right at the boundary of the computational domain. Since interest in aeroacoustics is invariably in the far field, an extrapolation of the solution from the outer boundary is usually required. From this standpoint the absorbing boundary conditions are not as useful. The asymptotic radiation boundary condition is, perhaps, most suitable for our purpose. The first-order Bayliss–Turkel radiation boundary condition for the Helmholtz equation may be written as

$$\frac{\partial p}{\partial r} - \left(ik - \frac{1}{2r}\right) p = 0. \tag{5}$$

The discretized form, to second-order accuracy, of (5) for a boundary point (m, n) with polar coordinates $(r_{m,n}, \theta_{m,n})$ is

$$\cos\theta_{m,n}\frac{(p_{m+1,n} - p_{m-1,n})}{2\Delta x} + \sin\theta_{m,n}\frac{(p_{m,n+1} - p_{m,n-1})}{2\Delta y} - \left(ik - \frac{1}{2r_{m,n}}\right) p_{m,n} = 0. \tag{6}$$

Equation (6) provides the value of p at the ghost point immediately outside the computational domain. At the corner points, where there are two adjacent ghost points, the values of p are assumed to be equal.

Equation (4) and boundary condition (6) form a closed system of algebraic equations. The matrix equation can easily be solved by a block tridiagonal algorithm for a given value of the parameter $\lambda/\Delta y$. Figure 1 shows the distribution of $|p|$ in the positive x-direction for a monopole source (Eq. (2)) at the origin. In the calculation a spatial resolution of 10 grid points per wavelength and a computational domain of 20×20 wavelengths were used. As can be seen the computed magnitude of $|p|$ generally decreases as x increases in accordance with the exact solution (see Eq. (3)) of the Helmholtz equaton. However, it is also apparent that the curve is not entirely smooth but has small amplitude modulations. A closer examination indicates that the amplitude modulations have a wavelength approximately equal to half of that of the original acoustic waves. The reason for the presence of small amplitude modulations is not difficult to find. Suppose the radiation boundary condition is not perfect so that for an outgoing wave e^{ikx} a very

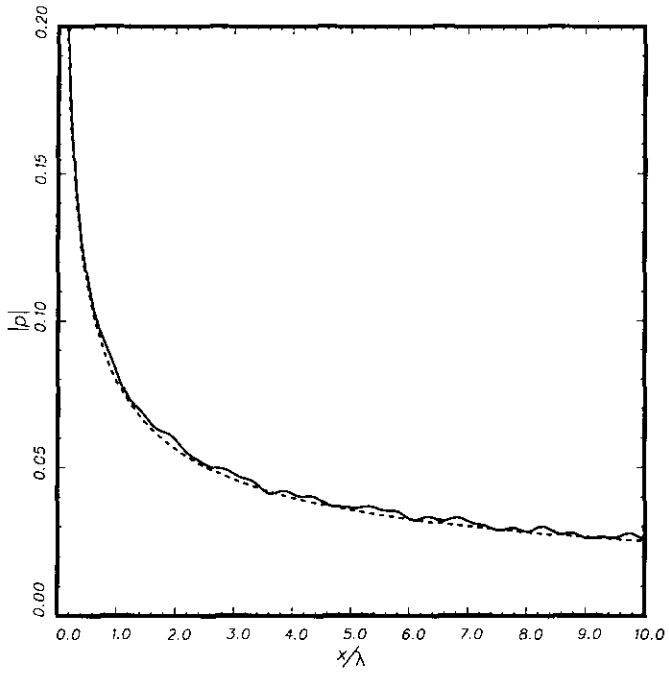

FIG. 1. Distribution of pressure intensity, $|p|$, along the x-axis. Monopole source at the origin. 10 grid points per wavelength: ——— computed solution; – – – exact solution.

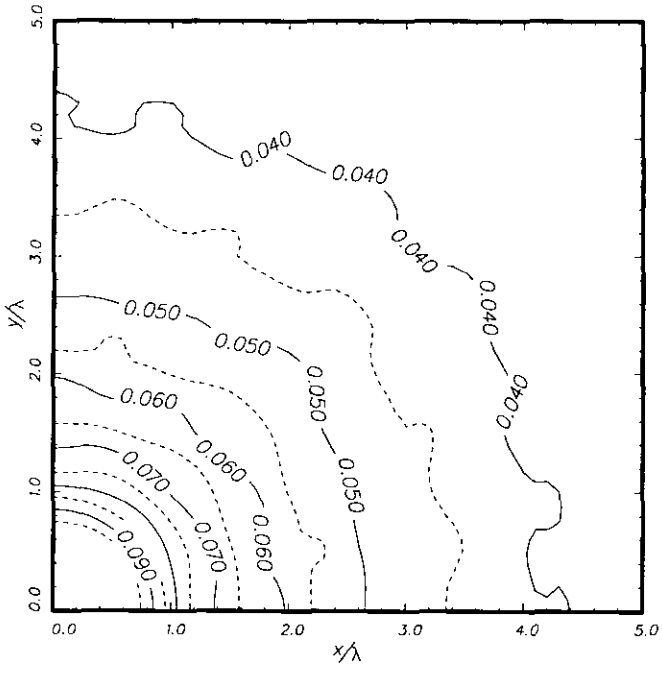

FIG. 2. Contours of equal sound intensity, $|p|$, in the x–y plane. Monopole source at the origin. 10 grid points per wavelength.

small reflected wave εe^{-ikx} ($\varepsilon \ll 1$) is created. The absolute magnitude of the combined outgoing and reflected waves is

$$|e^{ikx} + \varepsilon e^{-ikx}| = 1 + 2\varepsilon \cos(2kx) + O(\varepsilon^2). \tag{7}$$

Thus because of the small amplitude reflected wave there will be a small amplitude modulation of the total amplitude at half the wavelength of the original acoustic wave. Figure 2 shows the corresponding contour plot of $|p|$ (contours of equal sound intensity) in the $x-y$ plane. The deviations from circular contours are the results of very low amplitude reflections off the boundaries of the computational domain. Aside from creating relatively small reflected waves the Bayliss–Turkel radiation boundary condition appears to work quite well at a resolution of 10 grid points per wavelength. For many applications this could be satisfactory.

Now let us decrease $\lambda/\Delta y$ to 5, i.e., using a resolution of five grid points per wavelength in Eq. (4) and boundary condition (6), and recompute the result. The amplitude distribution as a function of x is shown in Fig. 3 and the contour plot in the $x-y$ plane is given in Fig. 4. At this low spatial resolution the reflected wave amplitude is no longer insignificant. Figures 3 and 4 bear no resemblance to that of the exact solution of the Helmholtz equation. It is not unreasonable to say that the Bayliss–Turkel radiation boundary condition creates excessive reflections and an improved radiation boundary condition is needed. It will be shown later that by using an improved radiation boundary condition a smooth numerical solution can be obtained.

In discussing the solution of wave propagation problems by finite-difference approximation, Vichnevetsky and Bowles [12] and Trefethen [13] noted that the phase and group velocities of the waves of the difference equation are anisotropic even though the same waves as described by

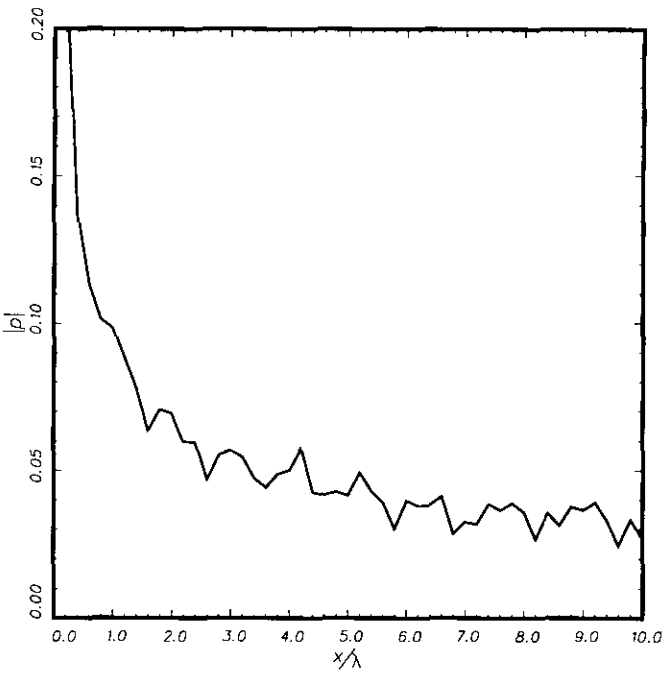

FIG. 3. Calculated distribution of pressure intensity, $|p|$, along the x-axis using the Bayliss–Turkel radiation boundary condition. Monopole source at the origin. Five grid points per wavelength.

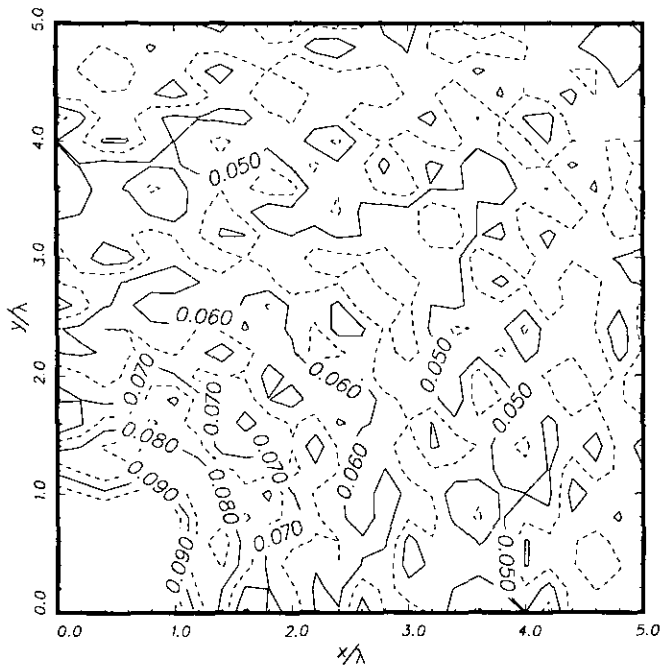

FIG. 4. Calculated contours of equal sound intensity, $|p|$, using the Bayliss–Turkel radiation boundary condition, in the x–y plane. Monopole source at the origin. Five grid points per wavelength.

the original partial differential equation are isotropic. Anisotropy in the group velocity leads immediately to distorted wave fronts. For the Helmholtz equation which provides a steady state response to time periodic forcing there are no clearly defined wave fronts. However, it will be demonstrated later that the computed wave amplitude is anisotropic. The amplitude anisotropic referred to here differs from that elaborated in [12, 13]. The degree of anisotropy depends strongly on the spatial parameter $\lambda/\Delta y$. For small $\lambda/\Delta y$ it can be quite large. If uncorrected it could even give misleading results.

The purpose of this paper is twofold:

(i) We propose an improved asymptotic radiation boundary condition for the solution of the Helmholtz equation in an open domain. The improved radiation boundary condition is to be effective even when low spatial resolution is used. Unlike the Bayliss–Turkel radiation boundary condition which is based on the asymptotic solution of the partial differential equation the present improved radiation boundary condition is developed from the asymptotic solution of the governing finite difference equation. It will be shown that because of the compatibility between the field equation and the improved radiation boundary condition, reflections are totally eliminated even when only five grid points per wavelength are employed in the computation scheme.

(ii) We will first describe the phenomenon of amplitude anisotropy in solving the Helmholtz equation by finite difference approximation. Then we will propose a way to correct this anisotropy. This is done by developing an anisotropy correction factor based on the asymptotic solution of the Helmholtz equation (1) and that of the finite difference equation (4). The correction factor is independent of the acoustic sources present. It can hence be determined once and for all.

In Section 2 an improved radiation boundary condition for use in conjunction with the finite difference solution of the Helmholtz equation will be developed. The phenomenon of anisotropy will be examined in Section 3. A correction factor will be developed and its effectiveness demonstrated. In order to show that the improved radiation boundary condition and anisotropy convection factor do work in problems with complex acoustic sources, the problem of acoustic wave diffraction by a flat plate of finite length placed adjacent to a monopole source is considered in Section 4.

2. IMPROVED RADIATION BOUNDARY CONDITION

Upon examining the monopole source problem in Section 1 closely it appears that the suggestion of Bayliss and Turkel of using the asymptotic solutions to construct a radiation boundary condition is basically sound. The excessive reflections observed at low spatial resolution are simply a case of incompatibility between the governing finite-difference equation and the asymptotic radiation boundary condition of the partial differential equation. The incompatibility becomes clear if one remembes that for a given frequency the wave number, the phase and group velocities of the finite difference equation (4), and those of the partial differential equation (1) are not the same [12, 13]. In other words, the wave number k in (5) is not equal to the effective wave number of the finite difference equation. To obtain compatibility we propose constructing an improved radiation boundary condition based on the asymptotic solution of the finite difference equation itself.

2.1 *Asymptotic Solution of Finite Difference Equation*

Consider the following finite difference equation of the continuous variables x and y:

$$\frac{\phi(x+\Delta x, y)-2\phi(x, y)+\phi(x-\Delta x, y)}{(\Delta x)^2} + \frac{\phi(x, y+\Delta y)-2\phi(x, y)+\phi(x, y-\Delta y)}{(\Delta y)^2} + k^2\phi(x, y)=f(x, y). \tag{8}$$

It is easy to see that the discrete finite difference equation (4) is a special case of (8). By selecting the subset $x = m\,\Delta x$, $y = n\,\Delta y$, where m, n are integers, Eq. (8) becomes Eq. (4). That is, the solution of Eq. (4) may be obtained by setting $x = m\,\Delta x$, $y = n\,\Delta y$ in the solution of Eq. (8). The function $\phi(x, y)$ depends continuously on x and y. Its Fourier transform $\tilde{\phi}(\alpha, \beta)$, where α and β are the Fourier transform variables is, therefore, well defined. The relationship between $\phi(x, y)$ and $\tilde{\phi}(\alpha, \beta)$ are

$$\tilde{\phi}(\alpha, \beta) = \frac{1}{(2\pi)^2} \iint_{-\infty}^{\infty} \phi(x, y)\, e^{-i(\alpha x + \beta y)}\, dx\, dy \tag{9a}$$

$$\phi(x, y) = \iint_{-\infty}^{\infty} \tilde{\phi}(\alpha, \beta)\, e^{i(\alpha x + \beta y)}\, d\alpha\, d\beta. \tag{9b}$$

It is to be noted that the Fourier transform of $\phi(x + \Delta x, y)$ is related to that of $\phi(x, y)$ by the multiplicative factor $\exp(i\alpha\,\Delta x)$, i.e.,

$$\frac{1}{(2\pi)^2} \iint_{-\infty}^{\infty} \phi(x + \Delta x, y)\, e^{-i(\alpha x + \beta y)}\, dx\, dy = e^{i\alpha \Delta x} \tilde{\phi}(\alpha, \beta). \tag{10}$$

By means of (10) the Fourier transform of (8) is

$$\left[\frac{(e^{i\alpha\Delta x} - 2 + e^{-i\alpha\Delta x})}{(\Delta x)^2} + \frac{(e^{i\beta\Delta y} - 2 + e^{-i\beta\Delta y})}{(\Delta y)^2} + k^2\right] \tilde{\phi}(\alpha, \beta) = \tilde{F}(\alpha, \beta), \tag{11}$$

where $\tilde{F}(\alpha, \beta)$ is the Fourier transform of the source function $f(x, y)$. On solving (11) for $\tilde{\phi}(\alpha, \beta)$ and by inverting the Fourier transform it is straightforward to find

$$\phi(x, y) = \iint_{-\infty}^{\infty} \left\{\tilde{F}(\alpha, \beta)\, e^{i(\alpha x + \beta y)} \Big/ \left[k^2 - \frac{4}{(\Delta x)^2} \sin^2\left(\frac{\alpha\,\Delta x}{2}\right) - \frac{4}{(\Delta y)^2} \sin^2 \frac{(\beta\,\Delta y)}{2}\right]\right\} \times d\alpha\, d\beta. \tag{12}$$

For convenience, we will assume that the angular frequency ω has a slight positive imaginary part (as in the Laplace transform), i.e., $\mathrm{Im}(\omega) \to 0^+$, so that the wave number k ($k = \omega/a_0$) in (12) also has a slight positive imaginary part. Define the function $\eta(\alpha)$ by

$$\eta(\alpha) \equiv \left[\sin^2\left(\frac{\alpha\,\Delta x}{2}\right) - k^2 \frac{(\Delta x)^2}{4}\right]^{1/2}. \tag{13}$$

The branch cuts of $\eta(x)$ in the complex α-plane are shown in Fig. 5. In terms of $\eta(\alpha)$ (12) may be rewritten as

$$\phi(x, y) = \frac{-(\Delta y)^2}{4} \iint_{-\infty}^{\infty} \left\{\tilde{F}(\alpha, \beta)\, e^{i(\alpha x + \beta y)} \Big/ \left[\sin\left(\frac{\beta\,\Delta y}{2}\right) + i\frac{\Delta y}{\Delta x}\eta(\alpha)\right] \times \left[\sin\left(\frac{\beta\,\Delta y}{2}\right) - \frac{i\,\Delta y}{\Delta x}\eta(\alpha)\right]\right\} d\beta\, d\alpha. \tag{14}$$

The integrand of (14) has a simple pole at β_+ in the upper half β-plane and a simple pole at β_- in the lower half β-plane, where

$$\beta_\pm = \mp \frac{2}{\Delta y} \sin^{-1}\left[i\frac{\Delta y}{\Delta x}\eta(\alpha)\right]. \tag{15}$$

On evaluating the β-integral of (14) by the *residue theorem* it is straightforward to find that

$$\phi(x, y) = \begin{cases} \dfrac{\pi}{2}\Delta x \displaystyle\int_{-\infty}^{\infty} \frac{\tilde{F}(\alpha, \beta_+)}{\eta(\alpha)\cos(\beta_+\,\Delta y/2)}\, e^{i(\alpha x + \beta_+ y)}\, d\alpha, \\ \qquad y > 0 \\ \dfrac{\pi}{2}\Delta x \displaystyle\int_{-\infty}^{\infty} \frac{\tilde{F}(\alpha, \beta_-)}{\eta(\alpha)\cos(\beta_-\,\Delta y/2)}\, e^{i(\alpha x + \beta_- y)}\, d\alpha, \\ \qquad y < 0. \end{cases} \tag{16}$$

In the far field where $r = (x^2 + y^2)^{1/2} \to \infty$ the α-integral of (16) may be evaluated asymptotically by the method of stationary phase [14]. Let (r, θ) be the polar coordinates,

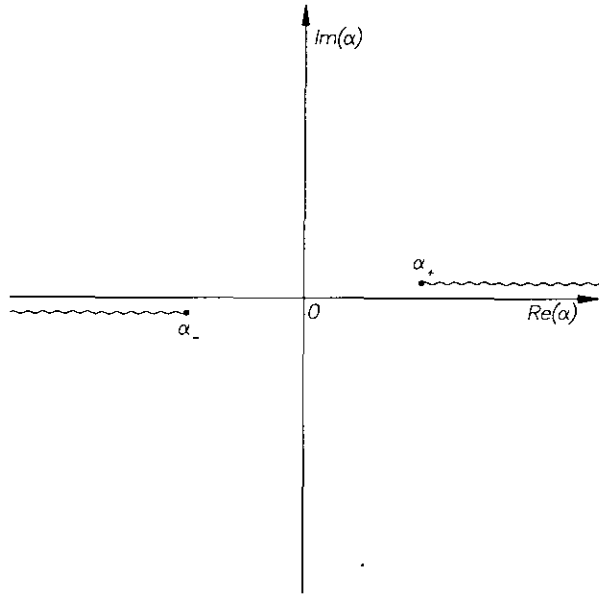

FIG. 5. Branch cuts of the function $\eta(\alpha)$ in the complex α-plane. $\alpha_\pm = \pm(2/\Delta x)\sin^{-1}(k\,\Delta x/2)$, $\mathrm{Im}(k) \to 0^+$.

where $x = r\cos\theta$, $y = r\sin\theta$. Equation (16) in the upper half-plane may be rewritten as

$$\underset{0<\theta<\pi}{\phi(r,\theta)} = \frac{\pi}{2}\Delta x \int_{-\infty}^{\infty} \frac{\tilde{F}(\alpha, \beta_+)\, e^{i(\alpha\cos\theta + \beta_+ \sin\theta)r}}{\eta(\alpha)\cos(\beta_+ \Delta y/2)}\, d\alpha. \quad (17)$$

For large r the stationary phase point of the α-integral at $\alpha = \alpha_s(\theta)$ is given by the roots of

$$\left.\frac{d\beta_+}{d\alpha}\right|_{\alpha=\alpha_s} = -\cot\theta. \quad (18)$$

Equation (18) has many roots. All but one are aliased roots. Here the aliased roots will be ignored. Upon evaluating the integral of (17) asymptotically for large r and retaining only the two lowest order terms in r^{-1} it is easy to find that

$$\underset{r\to\infty,\,0<\theta<\pi}{\phi(r,\theta)} = \frac{e^{iK(\theta)r}}{r^{1/2}}\left[G_0(\theta) + \frac{G_1(\theta)}{r}\right] + O\left(\frac{1}{r^{5/2}}\right), \quad (19)$$

where

$$K(\theta) = \alpha_s(\theta)\cos\theta + \beta_s(\alpha_s(\theta))\sin\theta \quad (20)$$

$$G_0(\theta) = \left[\frac{2\pi}{i\beta''_+(\alpha_s)\sin\theta}\right]^{1/2} \frac{\pi\,\Delta x}{2} \frac{1}{\eta(\alpha_s)\cos(\beta_+(\alpha_s)\,\Delta y/2)} \times \tilde{F}(\alpha_s, \beta_+(\alpha_s)). \quad (21)$$

For $\pi < \theta < 2\pi$ a similar asymptotic solution for $\phi(r,\theta)$ may be derived by using the second integral of (16). In (19) the explicit form of $G_1(\theta)$ can easily be found. It is not needed in the rest of this paper and, hence, will not be written out explicitly. Clearly in (19) the effective wave number is $K(\theta)$ and not k. Unlike k, $K(\theta)$ depends on the number of grid points per wavelength used as well as θ.

Now let $(r_{m,n}, \theta_{m,n})$ be the polar coordinates of the (m, n) point on the computation grid of the finite difference equation (4a). In the far field the asymptotic solution is obtained by replacing (r, θ) by $(r_{m,n}, \theta_{m,n})$ in (19). Thus

$$\underset{r_{m,n}\to\infty}{p_{m,n}} = \frac{e^{iK_{m,n}r_{m,n}}}{r_{m,n}^{1/2}}\left[G_0(\theta_{m,n}) + \frac{G_1(\theta_{m,n})}{r_{m,n}}\right] + O(r_{m,n}^{-5/2}), \quad (22)$$

where

$$K_{m,n} = K(\theta_{m,n}). \quad (23)$$

2.2. *Improved Radiation Boundary Condition*

We will first consider the construction of a radiation boundary condition at the upper boundary of the computation domain parallel to the x-axis as shown in Fig. 6. The boundary points are at $n = N$. The points in the row

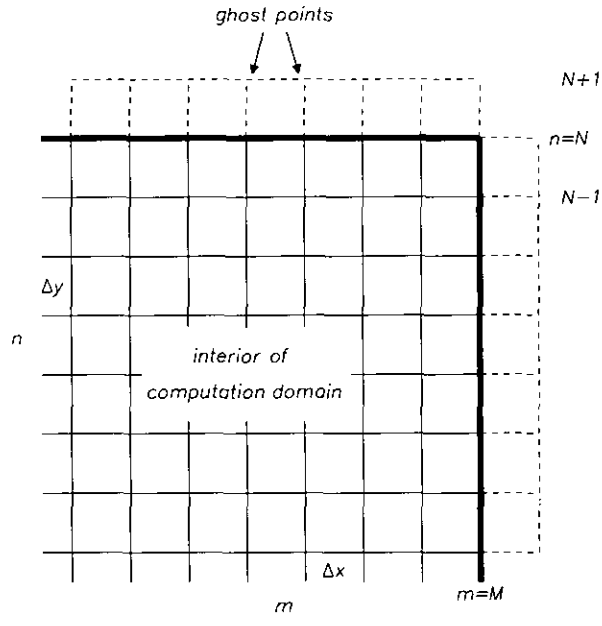

FIG. 6. Interior, boundary, and ghost points near the upper right-hand boundary of the computation domain.

$n = N+1$ are ghost points. The radiation boundary condition is to provide the values of $p_{m,N+1}$ in terms of the values at points inside and on the boundary of the computation domain.

Figure 7 shows the geometric relations between the ghost and interior points $(m, N+1)$ and $(m, N-1)$ and the boundary point (m, N). Let Δ be one-half of the distance

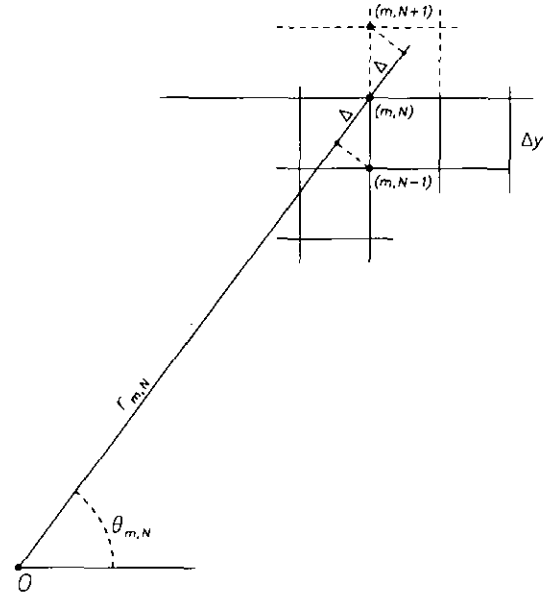

FIG. 7. Geometrical relations of the ghost and interior points $(m, N+1)$, $(m, N-1)$, and the boundary point (m, N).

between the projections of the points $(m, N+1)$ and $(m, N-1)$ on the radius vector $r_{m,N}$. Then

$$\theta_{m,N\pm1}=\theta_{m,N}\pm\frac{(\Delta y)\cos\theta_{m,N}}{r_{m,N}}\left(1\mp\frac{\Delta}{r_{m,N}}\right)+O(r_{m,N}^{-3}). \tag{24}$$

By straightforward expansion it is readily found that

$$G_0(\theta_{m,N\pm1})=G_0(\theta_{m,N})\pm G_0'(\theta_{m,N})\frac{(\Delta y)\cos\theta_{m,N}}{r_{m,N}}+O(r_{m,N}^{-2}) \tag{25}$$

$$\frac{G_1(\theta_{m,N\pm1})}{r_{m,N\pm1}}=\frac{G_1(\theta_{m,N})}{r_{m,N}}+O(r_{m,N}^{-2}),$$

where

$$G_0'=\frac{dG_0}{d\theta}.$$

Now by applying the asymptotic solution (22) of the finite difference equation to the three points $(m, N+1)$, (m, N), and $(m, N-1)$ it is easy to find after using (25) that

$$p_{m,N\pm1}=\frac{e^{iK_{m,N\pm1}r_{m,N\pm1}}}{r_{m,N\pm1}^{1/2}}\left[G_0(\theta_{m,N})\pm G_0'(\theta_{m,N})\times\frac{(\Delta y)\cos\theta_{m,N}}{r_{m,N}}+\frac{G_1(\theta_{m,N})}{r_{m,N}}\right]+O(r_{m,N}^{-5/2}) \tag{26}$$

$$p_{m,N}=\frac{e^{iK_{m,N}r_{m,N}}}{r_{m,N}^{1/2}}\left[G_0(\theta_{m,N})+\frac{G_1(\theta_{m,N})}{r_{m,N}}\right]+O(r_{m,N}^{-5/2}). \tag{27}$$

Finally by eliminating the right-hand sides of (26) and (27) the following radiation boundary condition for the upper boundary of the computation domain at $n=N$ is obtained:

$$p_{m,N+1}=2\left(\frac{r_{m,N}}{r_{m,N+1}}\right)^{1/2}e^{i(K_{m,N+1}r_{m,N+1}-K_{m,N}r_{m,N})}p_{m,N}-\left(\frac{r_{m,N-1}}{r_{m,N+1}}\right)^{1/2}e^{i(K_{m,N+1}r_{m,N+1}-K_{m,N-1}r_{m,N-1})}p_{m,N-1}. \tag{28}$$

For the computation boundaries parallel to the y-axis a similar radiation boundary condition may be constructed following the above procedure. For the right-hand boundary at $m=N$ the radiation boundary condition is

$$p_{M+1,n}=2\left(\frac{r_{M,n}}{r_{M+1,n}}\right)^{1/2}e^{i(K_{M+1,n}r_{M+1,n}-K_{M,n}r_{M,n})}p_{M,n}-\left(\frac{r_{M-1,n}}{r_{M+1,n}}\right)^{1/2}e^{i(K_{M+1,n}r_{M+1,n}-K_{M-1,n}r_{M-1,n})}p_{M-1,n}. \tag{29}$$

2.3. *Numerical Results*

To test the effectiveness of the improved radiation boundary conditions the fundamental solution of the Helmholtz equation is again considered. The numerical solution of the finite difference equation (4) with a monopole source on the right-hand side is recomputed using (28) and (29) as the boundary conditions. The distribution of $|p|$ in the x-direction at 10 grid points per wave length is shown (the solid curve) in Fig. 8. The broken curve in this figure corresponds to the exact solution. With the improved radiation boundary condition the calculated pressure amplitude distribution is smooth, totally free of reflections. Figures 9a and b show the calculated pressure distribution at five points per wave length in the x-direction and along a line at 45° to the x-axis. Again the computed curve is extremely smooth showing no sign of any reflection from the boundaries of the computation domain. A very careful examination of the smoothness of the entire computed solution has

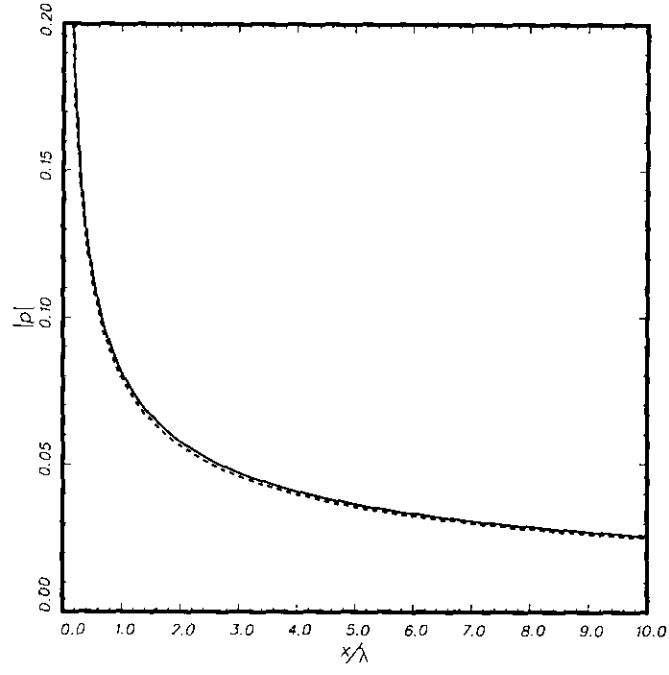

FIG. 8. Calculated pressure intensity, $|p|$, distribution along the x-axis. Monopole source at the origin. 10 grid points per wavelength: ——— improved radiation boundary condition; – – – exact solution.

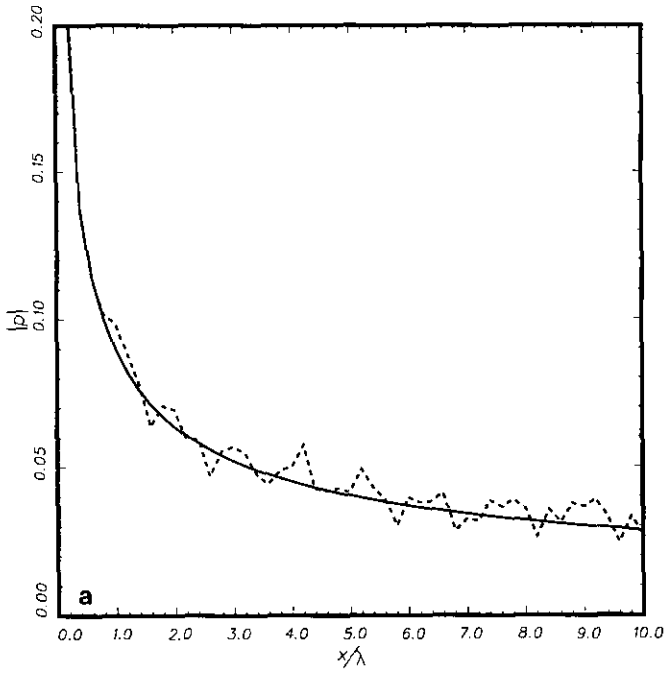

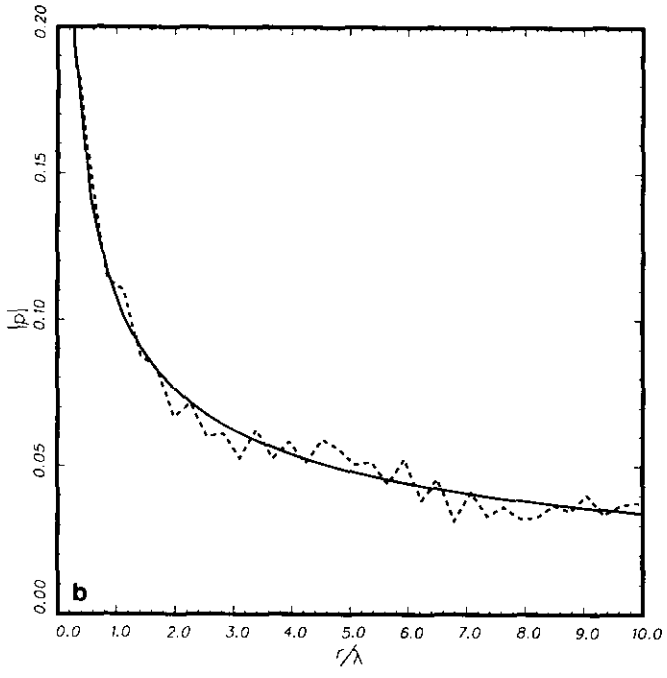

FIG. 9. (a) Calculated pressure intensity, $|p|$, distribution along the x-axis. Monopole source at the origin. Five grid points per wavelength. (b) Calculated pressure intensity, $|p|$, distribution along a line a 45° to the x-axis. Monopole source at the origin. Five grid points per wavelength: ——— improved radiation boundary condition; --- Bayliss–Turkel radiation boundary condition.

been carried out. No amplitude modulation can be detected indicating that the improved radiation boundary condition is, indeed, transparent to the outgoing acoustic waves.

3. ANISOTROPY

The use of finite difference approximation inevitably introduces anisotropy into the governing finite difference equation even though the Helmholtz equation itself is isotropic. On a square grid as shown in Fig. 6 the number of grid points per wavelength is the same in the x and y direction. However, the number of grid points per the same length will be less in any other directon. What this means is that when the number of grid points per wavelength is small the wave propagation characteristics are strongly direction dependent. To illustrate this point let us again consider the solution of finite difference equation (14) with a monopole nonhomogeneous source term. The improved radiation boundary condition is imposed at the boundaries of the computational domain. Figure 10 shows the calculated contours of equal sound intensity (equal $|p|$) in the first quadrant of the $x-y$ plane using five grid points per acoustic wavelength. Unlike Fig. 4 the contours are smooth, indicating the absence of reflections. However, the contours are not circular as the solution of the Helmholtz equation ought to be. The noncircular geometry of the contours is a direct consequence of the anisotropic characteristic of the governing finite difference equation.

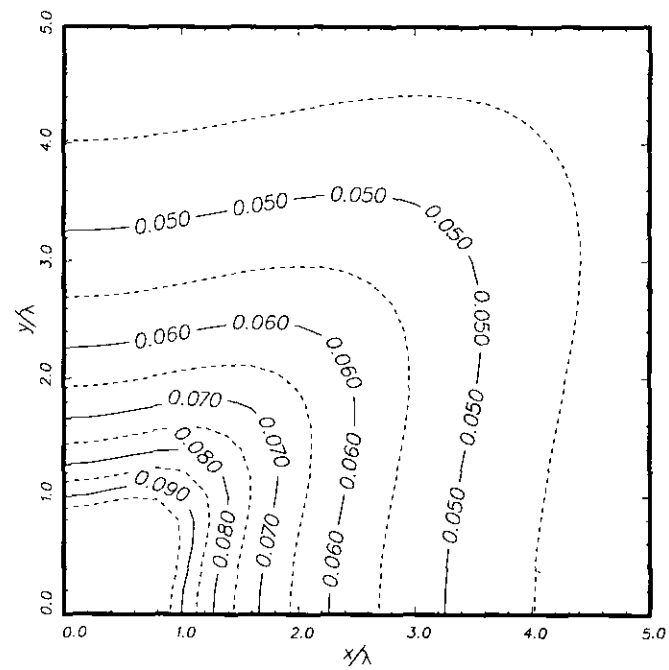

FIG. 10. Calculated contours of equal sound intensity, $|p|$, using the improved radiation boundary condition, in the x–y plane. Monopole source at the origin. Five grid points per wavelength.

The large effect of anisotropy in Fig. 10 renders the solution somewhat useless as an approximation to the solution of the Helmholtz equation. If one insists on using the finite difference equation (4), perhaps because of its simplicity, then, one way to make the solution useful is to develop a scheme to correct or cancel the effect of anisotropy. The possible existence of such a correction factor is not difficult to see since the finite difference equation (4) does contain many of the same essential wave propagation characteristics as the Helmholtz equation. The directional distribution is, however, distorted by the finite size rectangular grid. Clearly such a correction factor is a function of direction, θ, and the number of grid points per wavelength employed in the computation. However, the correction factor should not be source dependent. To construct such an anisotropy correction factor we propose using the asymptotic solutions of the finite difference equation (22) and the Helmholtz equation. By means of the method of Fourier transform the asymptotic solution of the Helmholtz equation is easily found to be

$$\underset{r\to\infty}{p(r,\theta)} = \left(\frac{2\pi}{k}\right)^{1/2} \frac{\pi}{ir^{1/2}} e^{i(kr-\pi/4)} \bar{F}(\bar{\alpha}_s, \bar{\beta}_+(\bar{\alpha}_s)) + O(r^{-3/2}), \tag{30}$$

where

$$\bar{\alpha}_s = k\cos\theta, \qquad \bar{\beta}_+(\bar{\alpha}_s) = k\sin\theta.$$

Equations (22) and (30) are similar in form. The pressure amplitude decays as $r^{-1/2}$ in both solutions. The ratio of the magnitudes of the leading terms of the two solutions (after cancelling out the source function) is

$$D(\theta, k\,\Delta x, k\,\Delta y) \equiv \frac{|p|_{\text{Helmholtz equation}}}{|p|_{\text{finite difference equation}}} = 2\,|\beta''_+(\alpha_s)|^{1/2}\,\eta(\alpha_s)\cos(\beta_+(\alpha_s)\,\Delta y/2) \times \sin^{1/2}\theta/(\Delta x\,|k|^{1/2}). \tag{31}$$

The quantity $D(\theta, k\,\Delta x, k\,\Delta y)$ is the sought-after anisotropy correction factor. It scales the finite difference solution to the solution of the Helmholtz equation. It is source independent. This correction factor can be calculated once and for all. Figure 11 shows the magnitude of the anisotropy correction factor as a function of θ at $\lambda/\Delta y$ ($\Delta x = \Delta y$) equal to 20, 15, 10, and 5. As can readily be seen the correction needed at five grid points per wavelength is quite large. Even at 15 grid points per wavelength a 3% correction is needed. Figure 12 shows the pressure amplitude contours of Fig. 10 corrected (multiplied) by the anisotropy correction factor of Fig. 11. The contours are now circular and are indistinguishable from the exact solution.

The anisotropy correction factor (31) is source independent. It is, therefore, applicable to all noise radiation problems irrespective of the complexity of the noise sources. To demonstrate this point the acoustic field generated by a fairly complicated source system will be considered in the next section.

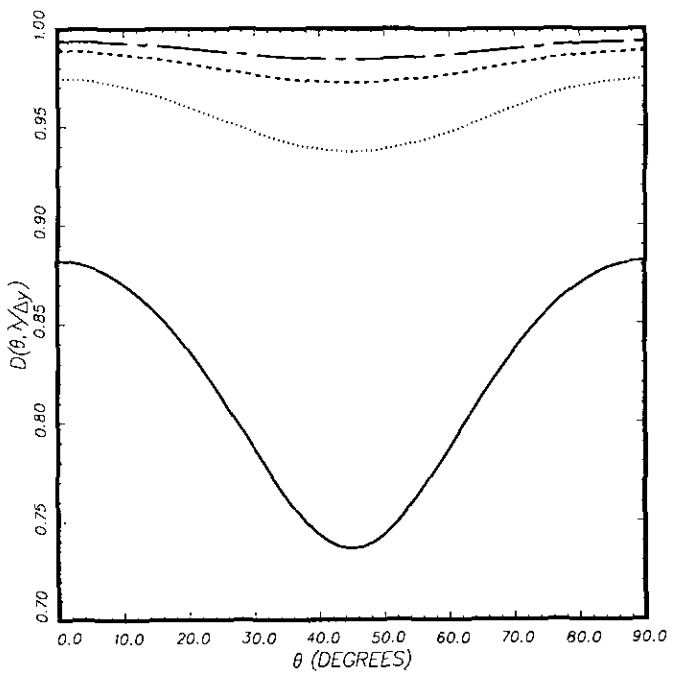

FIG. 11. Magnitude of anisotropy correction factor as a function of θ at $\lambda/\Delta y = 5$, 10, 15, and 20: —— $\lambda/\Delta y = 20$; – – – $\lambda/\Delta y = 15$; ····· $\lambda/\Delta y = 10$; —— $\lambda/\Delta y = 5$.

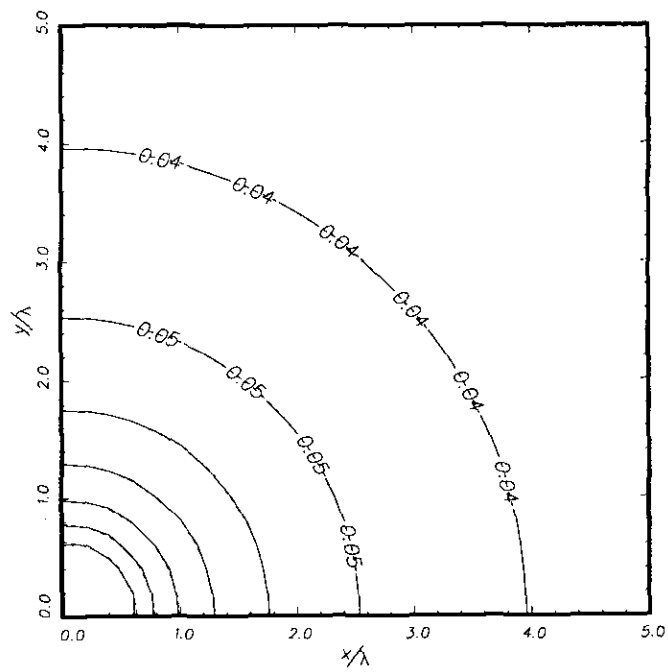

FIG. 12. Calculated contours of equal sound intensity, $|p|$, with anisotropy correction, in the x–y plane. Monopole source at the origin. Five grid points per wavelength: – – – exact solution.

4. SOURCE COMPLEXITY

The improved radiation boundary condition and anisotropy correction factor developed in Sections 2 and 3 are acoustic source independent. As such they are applicable even to problems involving sources of great complexity. In this section a concrete example of this kind will be given to illustrate the effectiveness of the improved radiation boundary condition and the anisotropy correction factor.

Let us consider the problem of acoustic wave diffraction by a flat plate as shown in Fig. 13. Here sound waves are generated by a monopole source located at a distance of two acoustic wavelengths from the plate. The flat plate is two acoustic wavelengths long. The flat plate reflects and diffracts the sound waves from the monopole source. On the back side of the plate, say along the computational boundary AB, the sound waves reaching there are mainly waves diffracted at the two sharp edges of the flat plate. Because the distances from the two edges are not the same the diffracted waves arriving at a point on AB would have a phase difference. If the phase difference is small the two diffracted waves would reinforce each other. If the phase difference is close to 180° they tend to cancel each other. In this way a diffraction pattern with maxima and minima is formed along AB.

The present acoustic wave diffraction problem can be solved exactly by separation of variables in an elliptic coordinate system centered on the flat plate. The exact solution will be used to compare with the numerical solution of finite difference equation (4). In the numerical solution the discretized boundary condition on the flat plate at $n = \bar{N}$ is

$$p_{m,\bar{N}+1} - p_{m,\bar{N}-1} = 0. \tag{32}$$

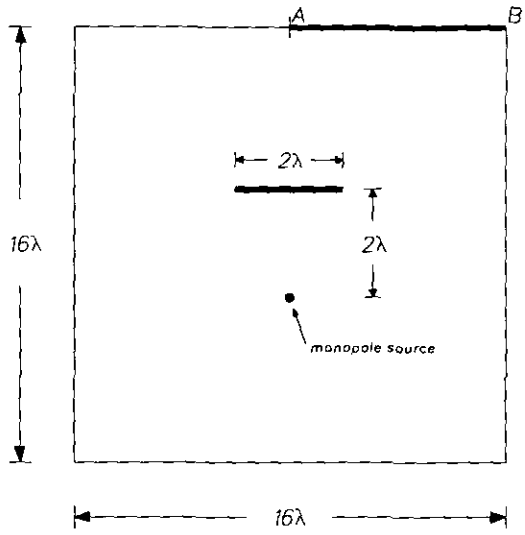

FIG. 13. Computation domain of an acoustic wave diffraction problem involving a monopole source and a flat plate. The origin of coordinates is located midway between the source and the plate.

Equation (32) corresponds to $\partial p/\partial y = 0$ to second-order accuracy.

The values $p_{m,\bar{N}}$ on the two sides of the plate are different. On the top side of the plate $(m, \bar{N}+1)$ is an interior point and $(m, \bar{N}-1)$ is a ghost point. The value of p at the ghost point is provided by (32). On the bottom side of the plate $(m, \bar{N}-1)$ is an interior point and $(m, \bar{N}+1)$ is a ghost point. Again the value of p at the ghost point is provided by (32). In applying the finite difference equation (4) to the left end point of the plate the value p at the first grid point to the right is taken to be the average of the two values of p on the two sides of the plate. Similar treatment is applied to the right end point of the plate.

Figure 14 shows the calculated pressure amplitude $|p|$ as a function of distance from A along AB using 10 grid points per wavelength. The curve labelled "uncorrected" represents the solution of the finite difference equation without anisotropy correction. The solution curve is smooth and free from amplitude modulation. This indicates that the improved radiation boundary condition is effective. The curve labelled "corrected" is obtained by multiplying the value of the uncorrected curve by the anisotropy correction factor of Fig. 11. As can easily be seen the corrected curve is generally closer to the exact solution. The largest correction is around the 45° directions where the corrected curve is nearly exact. Figure 15 shows a similar calculation at five grid points per wavelength. Even at this low spatial resolu-

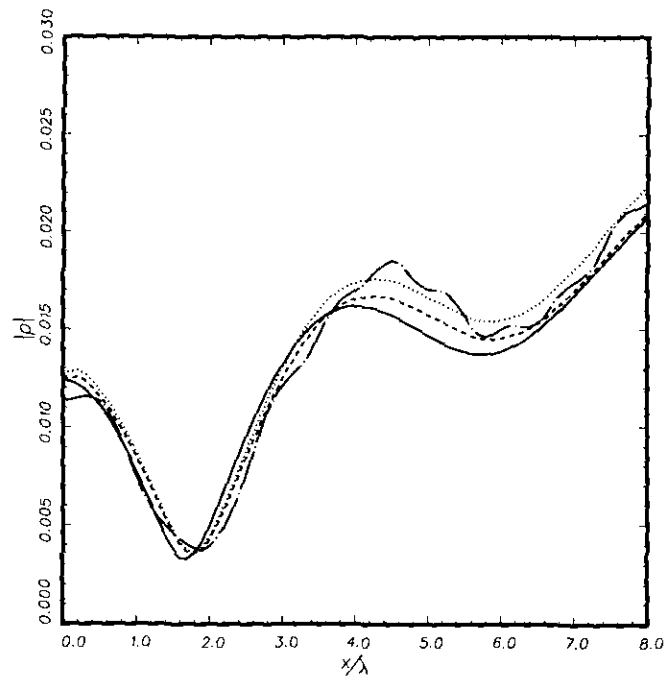

FIG. 14. Diffraction pattern along boundary AB of the computation domain. Ten grid points per wavelength: ——— exact solution; – – – solution with anisotropy correction; ····· uncorrected solution; — · — Bayliss–Turkel boundary condition.

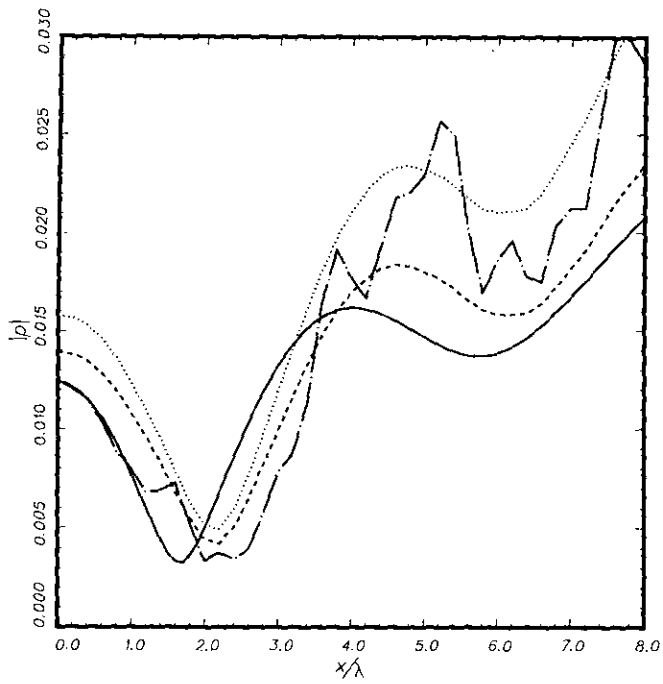

FIG. 15. Diffraction pattern along boundary AB of the computation domain. Five grid points per wavelength: ——— exact solution; – – – solution with anisotropy correction; ····· uncorrected solution; — — Bayliss-Turkel boundary condition.

tion the uncorrected curve is again free from reflections. However, it differs substantially from the exact solution. The use of the anisotropy correction factor greatly improves the accuracy of the solution. The greatest improvement is in the sector between $\theta = 45°$ to $70°$.

5. SUMMARY AND DISCUSSION

In this paper the radiation boundary condition for a finite difference equation used to approximate the Helmholtz equation is considered. It is found that an improved radiation boundary condition can be constructed starting from the asymptotic solution of the finite difference equation. Computed results indicate that the new radiation boundary condition yields essentially reflection free solutions even when a small number of grid points per wavelength is used. This is a significant improvement over the Bayliss–Turkel boundary condition which is based on the asymptotic solution of the partial differential equation. In section 3 the effectiveness of the improved radiation boundary condition has been demonstrated for the case of a simple source. In the course of this work the improved radiation boundary condition has also been applied to a number of problems involving more complex sources. They include the diffraction of acoustic waves from a monopole source by an adjacent thin plate of finite width, the case of two monopole sources, and a simple sourse embedded in a uniform stream (the convective wave equation is used in this case). In all these examples no reflection was observed when using as few as five grid points per wavelength. Because of space limitation we are unable to include these examples in the present paper.

The use of finite difference approximation inevitably introduces anisotropy into the solution. The effect of anisotropy can be quite large when the number of grid points per wavelength used in the computation is small. A way to correct this anisotropy is proposed. The correction factor is independent of the acoustic sources and for a given finite difference scheme can be computed once and for all. An example is provided to demonstrate the effectiveness of the anisotropy correction factor. Although not shown, the same anisotropic correction factor has been found to be just as effective for problems with fairly complicated noise sources. The improved radiation boundary condition and anisotropy correction factor constructed in the way described in Sections 1, 2, and 3 are also effective for higher order difference schemes and in problems with a uniform mean flow.

In this work, attention is focused primarily on correcting the amplitude of the computed solution. This is because for most aeroacoustics problems the sound intensity is the most important quantity. However, it must be pointed out that there are problems in which an accurate prediction of the relative phases of the acoustic waves in different directions is also important. For such problems a relative phase correction factor can be developed in a manner similar to that discussed in Section 3 by comparing the phases of the asymptotic solution of the finite difference equation and that of the partial differential equation. When both the amplitude and phase corrections are used then the finite difference computation amounts to essentially the determination of the Fourier transform of the source function. This should be an attractive strategy for some computational aeroacoustics problems, especially those with complex noise sources and with reflections and diffractions of the acoustic waves by solid bodies.

ACKNOWLEDGMENTS

This work was supported by the Office of Naval Research under Grant No. N00014-89-J-1836 and also in part by NASA Grant NAG 3-1267 and the Florida State University through time granted on its Cray-YMP Supercomputer.

REFERENCES

1. A. Bayliss and E. Turkel, *Commun. Pure Appl. Math.* **33**, 707 (1980).
2. A. Bayliss and E. Turkel, *J. Comput. Phys.* **48**, 182 (1982).

3. A. Bayliss, M. Gunzburger, and E. Turkel, *SIAM J. Appl. Math.* **42**, 430 (1982).
4. B. Engquist and A. Majda, *Math. Comput.* **31**, 627 (1977).
5. B. Engquist and A. Majda, *Commun. Pure Appl. Math.* **32**, 313 (1979).
6. R. L. Higdon, *Math. Comput.* **47**, 437 (1986).
7. R. L. Higdon, *Math. Comput.* **49**, 65 (1987).
8. H. Jiang and Y. S. Wong, *J. Comput. Phys.* **88**, 205 (1990).
9. R. Kosloff and D. Kosloff, *J. Comput. Phys.* **63**, 363 (1986).
10. K. W. Thompson, *J. Comput. Phys.* **68**, 1 (1987).
11. K. W. Thompson, *J. Comput. Phys.* **89**, 439 (1990).
12. R. Vichnevetsky and J. B. Bowles, *Fourier Analysis of Numerical Approximations of Hyperbolic Equations* (SIAM, Philadelphia, 1982).
13. L. N. Trefethen, *SIAM Rev.* **24**, 113 (1982).
14. R. Wong, *Asymptotic Approximations of Integrals* (Academic Press, New York, 1989), Chap. 3.
15. P. M. Morse and H. Feshbach, *Methods of Theoretical Physics* (McGraw–Hill, New York, 1953).